Role of Charge Transfer and Quinonoid Structure in the Raman Spectrum of Doped Poly(*p*-phenylene)

Lilee Cuff, Changxing Cui, and Miklos Kertesz*

Contribution from the Department of Chemistry, Georgetown University, Washington, D.C. 20057

Received January 25, 1994®

Abstract: We present an *ab initio* based, scaled quantum mechanical oligomer force field (SQMOFF) method for modeling the structure and vibrational spectra of doped poly(*p*-phenylene). By integrating this theoretical method and Raman spectroscopic technique, we are able to investigate quantitatively the structural evolution of poly(*p*-phenylene) upon doping. On the basis of our periodic quinonoid model and the observed inter-ring stretching frequency, we find heavily doped PPP to have only about 30% quinonoid character on the average. Accordingly, the average inter-ring C–C bond length decreases from 1.501 to 1.45(2) Å upon doping. This structural information, available for the first time, is fundamental in understanding the effects of doping. Additionally, we find that the corresponding force constant increases from 4.573 to 5.475 mdyn/Å upon doping. The intensity ratios of the four A_g modes are predicted by the SQMOFF method to be primarily dependent on the quinonoid structure of the doped polymer. The role of charge transfer in this context is primarily to increase the quinonoid character of the structure. A discussion on intensity ratios with respect to the effective conjugation coordinates theory is also presented.

Introduction

The discovery that conjugated organic polymers become highly conductive upon doping has fueled unprecedented research into the structure–conductivity relationship of these polymers.[1] The most extensively studied conjugated polymer is polyacetylene (PA), and an in-depth understanding of the relationship between its structure and charge transport process had led to the idea of soliton participation in the conduction mechanism.[2-6] Similar studies have been carried out on polymers whose ground states are not degenerate, e.g., polythiophene[7] (PT), polypyrrole[8] (PPy), and poly(*p*-phenylene)[9] (PPP), and the concept of polaron and bipolaron[10,11] as charge carriers has been invoked. It is believed that because these charge carriers could be delocalized in organic polymers (as opposed to ionic solids), conductivity at low dopant concentrations is mainly due to the mobility of these defects along the polymer chain.[12] However, the transport phenomenon at high dopant concentrations is not well understood. An inter-chain hopping mechanism has been proposed to be a plausible factor in the conductivity-limiting process.[13] In order to achieve a thorough understanding (rivaling that of PA) of the conducting mechanism of these polymers, much work has to be done relating structure to transport properties.

Because the structure of a highly doped polymer is a piece of the conduction mechanism puzzle, our study of conjugated polymer focuses on establishing a structure–spectrum relationship. Due to the difficulty in obtaining good crystals and therefore in carrying out an X-ray diffraction study, the geometries of most conducting polymers are relatively unknown, the bond lengths and bond angles in particular. However, vibrational spectroscopic methods are readily applicable to these polymers, pristine or doped. When combined with theoretical calculation, vibrational spectroscopic methods provide invaluable structural information. Resonance Raman spectroscopy is especially suited for studying conjugated polymers. This technique has been employed to study the dispersion of polymers[14,15] as well as to probe the presence of polarons and bipolarons.[16-19] In contrast to Raman spectra, IR spectra tend to be more complex and difficult to interpret. This is especially true for doped polymers, where the complexity is often compounded by the presence of broad dopant and Goldstone peaks.[4]

We recently completed a vibrational spectrum–structure investigation on pristine PPP. We were able to produce both IR and Raman spectra of pristine PPP closely resembling those obtained experimentally and established that pristine PPP is nearly planar (inter-ring torsional angle of about 10°).[20] In this study, we examine the structural and spectral evolution of PPP upon doping. We use our modeling method to complement experimental data in order to derive qualitative and quantitative information on the structure–spectrum relationship. It has been shown from quantum mechanical calculations[9,21] that the PPP ring structure changes from an aromatic to a more quinonoid form upon doping. This theoretical prediction is consistent with Raman spectra of doped PPP that show an upward shift in the inter-ring stretching frequency.[17,22-25] The IR spectra taken on

* Abstract published in *Advance ACS Abstracts*, August 15, 1994.

(1) *Handbook of Conducting Polymers*; Skotheim, T. A., Ed.; Dekker: New York, 1986; Vols. I and II. See Chapter 7, pp 213, regarding PPP.
(2) Su, W. P.; Schrieffer, J. R.; Heeger, A. J. *Phys. Rev. Lett.* **1979**, *42*, 1698.
(3) Su, W. P.; Schrieffer, J. R.; Heeger, A. J. *Phys. Rev.* **1980**, *B42*, 2099.
(4) Heeger, A. J.; Kievelson, S.; Schrieffer, J. R.; Su, W. P. *Rev. Mod. Phys.* **1988**, *60*, 781.
(5) Rice, M. J. *Phys. Lett.* **1979**, *A71*, 152.
(6) Roth, S.; Bleier, B. *Adv. Phys.* **1987**, *36*, 385.
(7) Chen, J.; Heeger, A. J.; Wudl, F. *Solid State Commun.* **1986**, *58*, 251.
(8) Scott, J. C.; Pfluger, P.; Krounbi, M. T.; Street, G. B. *Phys. Rev.* **1983**, *B28*, 2140.
(9) Bredas, J. L.; Chance, R. R.; Silbey, R. *Phys. Rev.* **1982**, *B26*, 5843.
(10) Brazovskii, S.; Kirova, N. *JETP Lett.* **1981**, *33*, 4.
(11) Bredas, J. L.; Chance, R. R.; Silbey, R. *Mol. Cryst. Liq. Cryst.* **1981**, *77*, 319.
(12) Fisher, A. J.; Hayes, W.; Wallace, D. S. *J. Phys.: Condens. Matter* **1989**, *1*, 5567.
(13) Kivelson, S. *Solitons*; North-Holland: Amsterdam, the Netherlands, 1986.
(14) Kurti, J.; Kuzmany, H. *Phys. Rev.* **1991**, *B44*, 597.
(15) Kurti, J.; Kuzmany, H. *Synth. Met.* **1992**, *49–50*, 665.
(16) Furukawa, Y.; Ohtsuka, H.; Tasumi, M.; Wataru, I.; Kanbara, T.; Yamamoto, T. *J. Raman Spectrosc.* **1993**, *24*, 551.
(17) Furukawa, Y.; Ohtsuka, H.; Tasumi, M. *Synth. Met.* **1993**, *55*, 516.
(18) Furukawa, Y.; Sakamoto, A.; Ohta, H.; Tasumi, M. *Synth. Met.* **1992**, *49*, 335.
(19) Sakamoto, A.; Furukawa, Y.; Tasumi, M. *J. Phys. Chem.* **1992**, *96*, 3870.
(20) Cuff, L.; Kertesz, M. *Macromolecules* **1994**, *27*, 762.
(21) Bredas, J. L.; Themans, B.; Fripiat, J. G.; Andre, J. M. *Phys. Rev.* **1984**, *B29*, 6761.
(22) Pelous, Y.; Froyer, G.; Herald, C.; Lefrant, S. *Synth. Met.* **1983**, *29*, E17.
(23) Krichene, S.; Lefrant, S.; Froyer, G.; Maurice, F.; Pelous, Y. *J. Phys.* **1983**, *44*, 733.
(24) Krichene, S.; Buisson, J. P.; Lefrant, S.; Froyer, G.; Maurice, F.; Goblot, J. Y.; Pelous, Y.; Fabre, C. *Mol. Cryst. Liq. Cryst.* **1985**, *118*, 301.

0002-7863/94/1516-9269$04.50/0

doped PPP are complex, having four new peaks on top of a broad band.[26,27] These peaks were attributed to doped PPP, but no correlation with structural change was deduced. Among the theoretical calculations are those carried out by Zannoni and Zerbi,[28] Lefrant and Buisson,[25] and Rakovic et al.[29] based on dynamical methods. These research groups had different objectives than ours. Zannoni and Zerbi presented their calculated frequencies of pristine PPP to be in reasonable qualitative agreement with experimental data. They also attempted to predict the change in vibrational frequencies with geometry modification; however, no definitive structure–spectrum relationship was established. On the other hand, Lefrant and Buisson reported mainly normal mode assignments and force constants of pristine and doped PPP. They were unable to reproduce the 1240 cm^{-1} band observed in the doped PPP Raman spectrum. In both cases, the inability to obtain a better fit was most likely due to difficulties in estimating the vast number of force constants, especially the off-diagonal coupling terms, required for dynamical calculations.

We envisage that knowledge gained in this study (on PPP) will induce a better understanding of many other conjugated polymers having an aromatic ring in the backbone, notably newly synthesized long-chain PPP[30] and planarized PPP.[31,32]

Computational Methods

We use the scaled quantum mechanical oligomer force field (SQMOFF) method to model an infinite polymer chain. Detailed description of this method can be found elsewhere.[33] In this section, we present a synopsis of the SQMOFF method.

In order to solve the Wilsonian GF matrix[34] for eigenvalues (vibrational frequencies) and eigenvectors (normal mode displacements), we use a k-dependent force matrix $\mathbf{F}(k)$ of the polymer that is expressed as[35]

$$\mathbf{F}(\mathbf{k}) = \mathbf{F}(0) + \sum_j \mathbf{F}(j) \exp(ikja)$$

where $\mathbf{F}(0)$ is the force matrix of the central unit of an oligomer. $\mathbf{F}(j)$ is the coupling force matrix between the central unit and its jth neighbor. Depending on the size of the repeat unit and the extent of delocalization, a trimer or pentamer is used. When a trimer is used, only the first neighbor interactions are included; pentamer is used when second neighbor interactions are significant. The k vector is the reciprocal lattice vector in the first Brillouin zone. In addition, dipole moment and polarizability derivatives, taken with respect to Cartesian coordinates of the central unit of the oligomer, are used to calculate IR intensities and Raman scattering activities of the polymer. All calculations on the oligomer are carried out at the *ab initio* level using the SCF Hartree–Fock method.

Since SCF Hartree–Fock calculations systematically overestimate force constants,[36] it is necessary to scale the force constants of the oligomer with a set of empirically determined scaling factors. These scaling factors are usually transferred from the monomer or a molecule similar to the repeat unit of the oligomer. The most commonly used nonuniform scaling procedure is that proposed by Pulay.[37] This scaling scheme required that internal coordinates be used in order to facilitate transferring of scaling factors—of similar bond type—between different molecules. Excellent transferability of scaling factors has been demonstrated in molecules. This feature is essential for the numerous successful applications of SQMOFF method in predicting the dynamical behavior of polymers,[33,38-43] including pristine PPP[20] at the double-ζ quality 3-21G basis set level. We have adopted the 3-21G basis set for the present doped PPP calculations. Discussion of the specific choices of scaling factors is given in the Results and Discussion section.

Structural Modeling of Highly Doped PPP. Conducting polymers undergo significant geometrical changes upon doping within the polymer backbone.[4] Whether the highly doped phases contain rather uniform polymer backbones exhibiting metallic behaviors or the solitonic/bipolaronic structures characteristic of the low dopant regime are maintained well into the highly doped regime is still a subject of debate. This offers two alternative approaches to model highly doped PPP: (a) a nonperiodic model incorporating bipolaronic local defects and (b) a periodic model which either represents an average structure of a nonperiodic material or is perhaps a realistic representation of the metallic phase.

The current paper is based on the second approach (b). We have three reasons for adopting this periodic model. First, the computational technique we have developed and applied successfully to the undoped periodic models of PPP is easily applied to periodic models of the doped phase. Second, upon doping, the spectrum of PPP changes markedly, as discussed in the remainder of the paper; the observed spectrum of the doped phase develops shifted vibrational bands, while the bands of the undoped phase disappear in some experiments. Third, the vibrational simulation based on the periodic model is quite successful, as shown in this paper.

In the remainder of this section we discuss the choices we made in developing the periodic model for the highly doped phase of PPP. As required by the SQMOFF method, oligomers of appropriate size have to be considered first. The method uses the optimized geometries and force constants of these oligomers to construct the dynamical matrix of the periodic polymer. For undoped PPP, the middle phenyl of terphenyl was used as the casting for generating the periodic infinite model.

Figure 1 depicts the three models we set up to study highly doped PPP. Terphenyls with two electrons added or removed are marked **Q(2-)** and **Q(2+)**, respectively. In addition, we also constructed a third model using a hypothetical molecule marked **Q** as the "pure" quinonoid model. This molecule is essentially a terphenyl capped with two methylene end groups in order to induce a quinonoid structure. We will compare these three models in terms of their vibrational frequencies and intensities. One of the conclusions of this comparison is that the influence of quinonoid structure in itself is more important than charge transfer in affecting the vibrational modes of both the n- and the p-type doped PPP. These choices are consistent with general chemical experience and calculations of Bredas et al.,[21] who estimated a charge transfer of 0.9 electrons per Na atom. The use of terphenyl is a compromise between cost and accuracy. While experimental data[16,17] and theoretical predictions[9,21] suggested that bipolarons could spread over 4–6 repeat units, *ab initio* calculations based on these larger oligomers are still prohibitively expensive at the moderate basis set level.

Geometry optimization and vibrational frequencies calculations on all three trimers are carried out at the 3-21G basis set level using the Gaussian 92 *ab initio* program.[44] The scaling factors used on these trimers are listed in Table 1. They are transferred from butadiene,[45] benzene,[20] and biphenyl.[20] The scaling factors of C—C and C=C (intra- and inter-

(25) Lefrant, S.; Buisson, J. P. *Organic Molecules for Nonlinear Optics and Photonics*; Kluwer Academic: the Netherlands, 1991.
(26) Schaklette, L. W.; Eckhart, H.; Chance, R. R.; Miller, G. G.; Ivory, D. M.; Baughman, R. H. *J. Chem. Phys.* **1980**, *73*, 4098.
(27) Yli-Lahti, P.; Stubb, H.; Isotalo, H.; Kuivalainen, P.; Kalervo, L. *Mol. Cryst. Liq. Cryst.* **1985**, *118*, 305.
(28) Zannoni, G.; Zerbi, G. *J. Chem. Phys.* **1985**, *82*, 31.
(29) Rakovic, D.; Bozovic, I.; Stepanyan, A.; Gribov, L. A. *Solid State Commun.* **1982**, *43*, 127.
(30) Gin, D. L.; Conticello, V. P.; Grubbs, R. H. *J. Am. Chem. Soc.* **1992**, *114*, 3167.
(31) Scherf, U.; Bohnen, A.; Mullen, K. *Makromol. Chem.* **1992**, *193*, 1127.
(32) Scherf, U.; Mullen, K. *Polymer* **1992**, *33*, 2443.
(33) Cui, C. X.; Kertesz, M. *J. Chem. Phys.* **1990**, *93*, 5257.
(34) Wilson, E. G., Jr.; Decius, J. C.; Cross, P. C. *Molecular Vibrations*; McGraw-Hill: New York, 1955.
(35) Painter, P. C.; Coleman, M. M.; Koenig, J. L. *The Theory of Vibrational Spectroscopy and its Applications to Polymer*; Wiley: New York, 1982.
(36) Pople, J. A.; Schlegel, H. B.; Krishnan, R.; Defrees, D. J.; Binkley, J. S.; Frisch, M. J.; White, R. A.; Hout, R. F.; Hehre, W. J. *Int. J. Quantum Chem. Quantum* Chem. *Symp.* **1981**, *15*, 267.
(37) Pulay, P.; Fogarasi, G.; Boggs, J. E.; Vargha, A. *J. Am. Chem. Soc.* **1983**, *105*, 7037.
(38) Cui, C. X.; Kertesz, M.; Dupuis, M. *J. Chem. Phys.* **1990**, *93*, 5890.
(39) Cui, C. X.; Kertesz, M.; Eckhardt, H. *Synth. Met.* **1991**, *41–43*, 3491.
(40) Kofranek, M.; Kovar, T.; Karpfen, A.; Lishka, H. *J. Chem. Phys.* **1992**, *96*, 4464.
(41) Kofranek, M.; Kovar, T.; Lishka, H.; Karpfen, A. *J. Mol. Struct.* **1992**, *259*, 181.
(42) Eckhardt, H.; Baughman, R. H.; Buisson, J. P.; Lefrant, S.; Cui, C. X.; Kertesz, M. *Synth. Met.* **1991**, *43*, 3413.
(43) Cuff, L.; Kertesz, M.; Geisselbrecht, J.; Kurti, J.; Kuzmany, H. *Synth. Met.* **1993**, *55*, 564.
(44) Frisch, M. J.; Head-Gordon, M.; Trucks, G. W.; Gill, P. M. W.; Wong, M. W.; Foresman, J. B.; Johnson, B. G.; Schlegel, H. B.; Robb, M. A.; Replogle, E. S.; Gomperts, R.; Andres, J. L.; Raghavachari, K.; Binkley, J. S.; Gonzalez, C.; Martin, R. L.; Fox, D. J.; Defrees, D. J.; Baker, J.; Stewart, J. J. P.; Pople, J. *Gaussian 92*; Gaussian Inc.: Pittsburgh, PA, 1992.
(45) Cuff, L. Unpublished work.

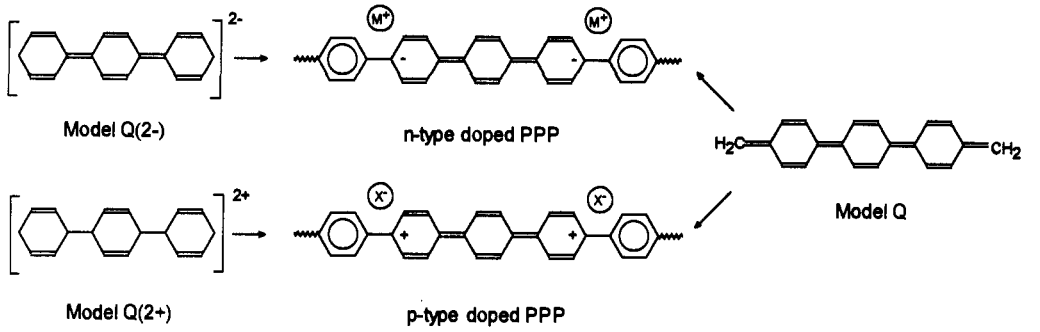

Figure 1. Three models, Q(2–), Q(2+), and Q, used in this study. Models Q(2–) and Q(2+) are based on terphenyl dianion and dication, respectively. The Q model is based on a hypothetical molecule which is essentially a terphenyl capped with CH_2 at both ends in order to induce a quinonoid structure.

Table 1. Scaling Factors and Force Constant of Doped PPP (Model Q)

	doped PPP			
	this work		ref 46	pristine PPP
description	scaling factors[a]	force constants	force constants	ref 20 force constants
C—C inter-ring stretch	0.6000[b]	5.475	5.05	4.573
C—C stretch	0.9818[c]	5.455	4.38	6.610[d]
C=C stretch	0.7830[c]	8.111	7.53	
C—H stretch	0.8279	5.284		
C—H in-plane deformation	0.7666	0.535		
C—C in-plane deformation	0.9950	1.544		
C—H wag	0.7134	0.386		
C—C inter-ring wag	0.7848	0.424		
ring deformation	0.7438	1.064		
		1.072		
		1.064		
ring torsion	0.7367	0.224		
		0.223		
		0.224		
inter-ring torsion	0.9904	0.058		
CC/CC coupling	0.6912			

[a] All scaling factors are identical to those used for pristine PPP (ref 20) unless otherwise stated. [b] Best fit to experimental spectrum. [c] Values from butadiene. [d] Average of six intra-ring C–C stretching force constants.

ring) stretches are transferred from butadiene; all other scaling factors are transferred from benzene and biphenyl and are identical to those used for pristine PPP. All these parameters are fixed except the inter-ring scaling factor, which is varied to fit the experimental Raman spectrum. Internal coordinates used are the same as those used in modeling PPP.[20]

Results and Discussion

Comparison of Q(2–), Q(2+), Q Models. The optimized geometries of the Q(2–), Q(2+), and Q trimers are shown in Figure 2. The main geometrical difference between these three models is the inter-ring C–C bond length. The values are 1.388, 1.388, and 1.365 Å for the Q(2–), Q(2+), and Q models, respectively. While the Q(2–) and Q(2+) forms have the same inter-ring C–C bond lengths, model Q has a distinctively shorter one. This shorter C–C bond lengh of model Q, as we shall see later, will result in an overestimation of the inter-ring stretching frequency.

The calculated unscaled vibrational frequencies of doped PPP based on Q(2+), Q(2–), and Q models are shown in Figure 3. It can be seen that all three models produce similar frequency patterns. In particular, the especially close resemblance of the frequency patterns of the Q(2+) and Q(2–) models is consistent with the structural similarity of their repeat units.

The calculated Raman spectra showing the four A_g modes (whose intensities are the highest) are shown in Figure 4. It can be seen that the Q(2+) and Q(2–) models, despite their difference

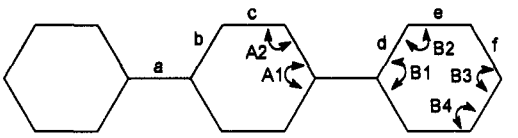

	Q(2-)	Q	Q(2+)
Bond Lengths			
a	1.3879	1.3650	1.3881
b	1.4636	1.4575	1.4622
c	1.3425	1.3345	1.3332
d	1.4563	1.4641	1.4418
e	1.3660	1.3307	1.3593
f	1.4012	1.4626	1.4008
Angles			
A1	112.031	113.752	115.238
A2	123.985	123.124	122.381
B1	112.418	114.499	116.843
B2	122.841	122.851	121.223
B3	122.907	122.390	119.797
B4	115.904	115.020	121.118

Figure 2. 3-21G basis set optimized geometries of terphenyl dianion Q(2–), dication Q(2+), and model trimer Q.

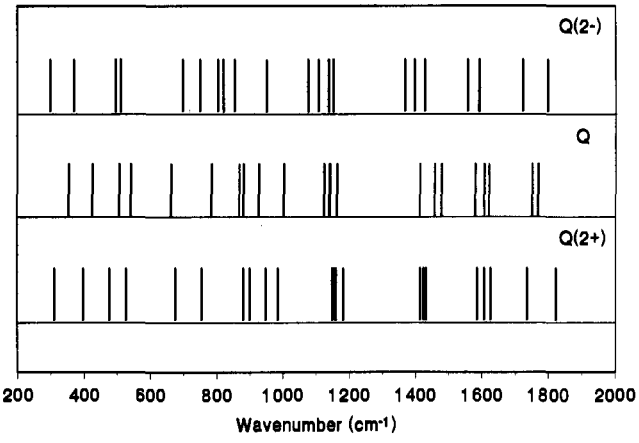

Figure 3. Calculated vibrational frequencies (unscaled) of doped PPP. All three models yield similar patterns, with a slight difference for the Q model.

in charges, give similar Raman spectra in terms of frequency and intensity. This can be attributed to their similar geometries. On the other hand, the Q model yields a slightly different pattern, notably a higher inter-ring stretching frequency (peak B in Figure 4) and a higher peak B:peak C intensity ratio (I_B/I_C). These results show that (1) there is no significant difference in the Raman spectra of n- and p-type doped PPP and (2) the intensity ratios of the four Raman-active bands are dependent primarily on the quinonoid structure. The role of charge transferred in this context is primarily to induce the structural change, which in turn leads to changes in the polarizability derivatives.

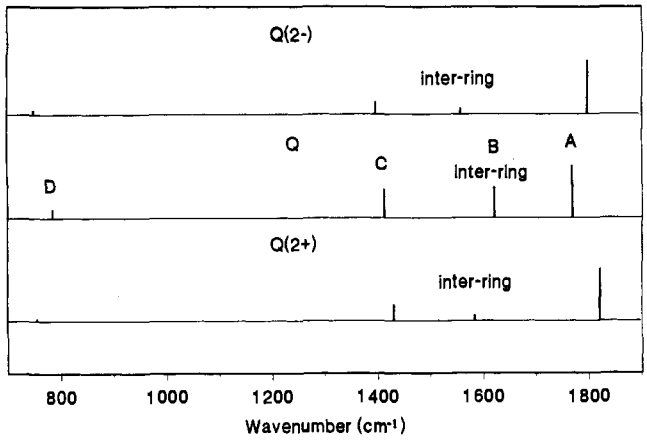

Figure 4. Calculated Raman spectra (unscaled) of doped PPP. The ordinates show the relative intensity of four A_g modes.

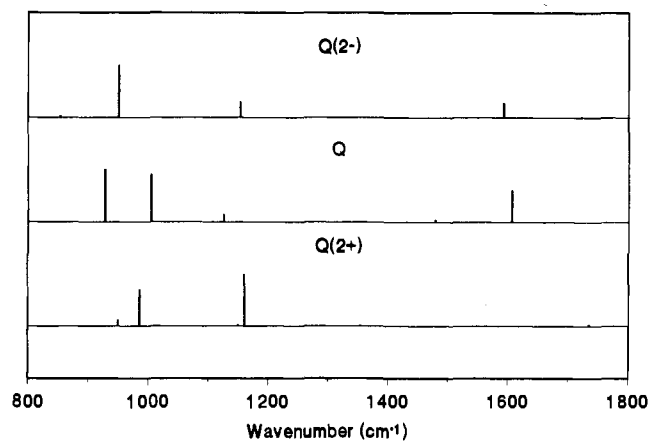

Figure 5. Calculated IR spectra (unscaled) of doped PPP. All three spectra show different patterns due to intensity difference.

Figures 5 depicts the calculated IR spectra, which are significantly different in appearance due to intensity differences. With the paucity of well-resolved IR spectra, we are unable to conclude whether any one model is better than the others.

From the above results, we note that either **Q(2+)** or **Q(2–)** could be used to model doped PPP, while the **Q** model could be used to determine the quinonoid contribution to the vibrational spectrum. Further, experimental data show that Raman, not IR, spectra of doped PPP are better suited for our purpose because they comprise well-resolved peaks and significant inter-ring stretching frequency shift. In the next section, we will focus on the use of model **Q** in studying the Raman spectrum and structure of doped PPP.

Spectrum and Structure of Doped PPP. In this section, our discussion will be based on model **Q**; similar inferences could be made for both the **Q(2–)** and the **Q(2+)** models.

After scaling with scaling factors transferred from benzene and butadiene, the inter-ring stretching frequency of the **Q** model is found to be significantly higher than that observed by Raman spectroscopy. This is attributed to the "pure" quinonoid structure adopted in this model. Putting it in another perspective, it could be said that the structure of doped PPP is not purely quinonoid.

Comparison between experimental Raman spectra of pristine and doped PPP shows that the inter-ring stretching frequency increases significantly upon doping. This increase is consistent with the bipolaronic picture, which requires an increase in the quinonoid character of the inter-ring C–C bond. Therefore, we take the inter-ring stretching frequency as a measure of the quinonoid character of doped PPP. Now, we present two independent approaches that allow us to deduce the inter-ring C–C bond length and the fraction of quinonoid character present in doped PPP.

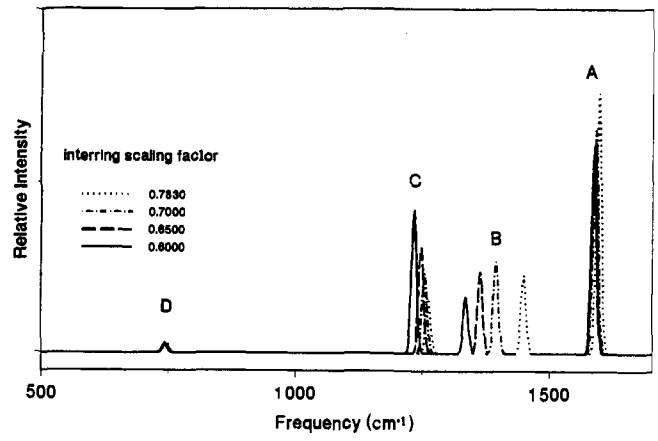

Figure 6. Changes in the frequencies and intensities of the four A_g modes with varying inter-ring C–C stretching scaling factors of model **Q**. While the inter-ring C–C stretching frequency decreases significantly with decreasing scaling factors, the other three remain largely unaffected. It is interesting to note that the intensity ratio of the 1330 and 1240 cm^{-1} bands also changes with scaling factor.

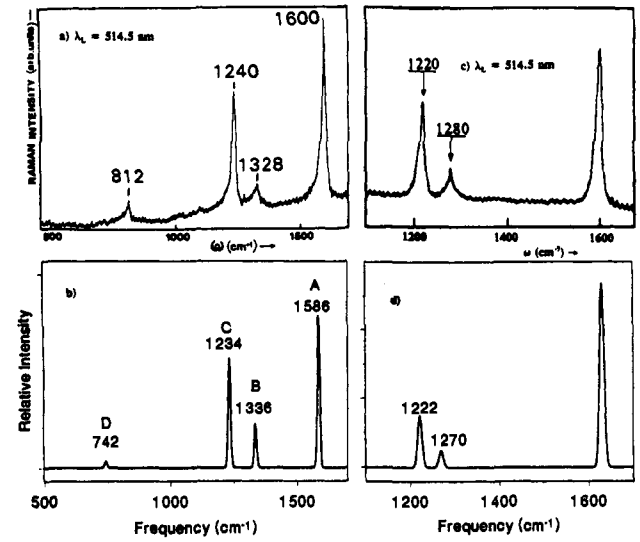

Figure 7. Comparison between the experimental and calculated Raman spectra of PPP. (a) Raman spectrum of doped electropolymerized[55] PPP (reproduced with permission from ref 22). The 812 cm^{-1} band seen in this Raman spectrum is not predicted by all three models and not observed in other experimental Raman spectra. (b) Simulated Raman spectrum of doped PPP: model **Q**, inter-ring C–C stretch scaling factor, 0.6000. (c) Raman spectrum of pristine electropolymerized PPP[50] (reproduced with permission from ref 46). (d) Calculated Raman spectrum of pristine PPP (inter-ring torsional angle, 20°; refer also to ref 20).

In our first approach, we fit the Raman spectrum obtained by Pelous et al.[22] by varying the inter-ring scaling factor. (This experimental spectrum is used because the sample consists of longer chains and is heavily doped. These are important factors because our model is a heavily doped infinite chain.) We progressively decrease the inter-ring scaling factor from 0.7830 (value from butadiene) to 0.7000, 0.6500, and 0.6000. From Figure 6, it can be seen that only the inter-ring stretching mode (peak B) shifts toward lower frequency, while the other A_g modes are not significantly affected. This observation is indicative of very little coupling between these modes and the inter-ring stretching mode. In addition, the intensity ratio of peak B:peak C (I_B/I_C) decreases from 1.39 to 0.39. The decreases both in inter-ring stretching frequency and I_B/I_C ratio give rise to a better agreement with experimental results.

As indicated by Figure 7 and Table 2, the use of an inter-ring scaling factor of 0.6000 produces a Raman spectrum in good agreement with experiment. However, the 812 cm^{-1} peak observed in this experimental spectrum[22] is not predicted by our calculations

Table 2. Calculated (Scaled Model Q) and Experimental Vibrational Frequencies (cm^{-1}) and Intensities[a] of Doped PPP

	calculated					
	this work			experiment[b]		
symmetry	frequency	intensity	ref 25 frequency	ref 22 frequency	ref 25 frequency	ref 17 frequency
			In-Plane Modes Raman-active			
A_g	1586	117114	1600	1600 (vs)	1595 (vs)	1586 (vs)
	1336	33053	1320	1328 (m)	1322 (w)	1344 (m)
	1234	83795	1212	1240 (s)	1240 (s)	1220 (mw)
	742	4988	741	812 (w)		
B_{3g}	1470	294				
	1313	26.6				
	592	11.7				
	496	12.4				
IR active						
B_{1u}	1437	65.9				
	991	4.97				
	948	73.0				
B_{2u}	1589	0.00				
	1324	3.26				
	1118	0.37				
			Out-of-Plane Modes Raman active			
B_{1g}	732	8.59				
B_{2g}	963	264				
	763	346				
	305	1.22				
IR active						
B_{3u}	785	87.1				
	367	18.7				
nonactive						
A_u	964	0.00				
	444	0.00				

[a] IR intensities in km/mol, Raman scattering activity in Å⁴/amu. [b] Intensities are described in parentheses. v, very; s, strong; m, medium; w, weak.

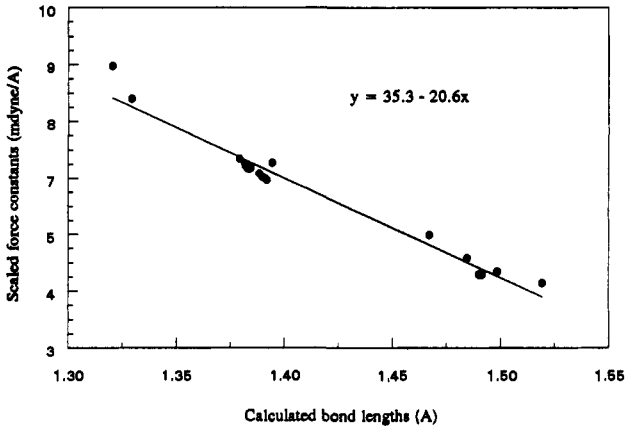

Figure 8. Plot of scaled force constants and bond lengths calculated at the 3-21G basis set level. Data are taken from butadiene, benzene, biphenyl, and terphenyl (see text).

(all three models). Furthermore, this peak is also not observed in all other Raman spectra.[16,17,23,24] Therefore, we are uncertain if the origin of this peak is doped PPP.

The inter-ring stretching force constant obtained with this scaling factor is 5.475 mdyn/Å. We estimate that this force constant corresponds to a bond length of 1.45(2) Å. This bond length is obtained by using a plot of scaled force constants vs bond lengths (see Figure 8). The bond lengths in this diagram are those of butadiene, benzene, biphenyl, and terphenyl calculated using the 3-21G basis set. The corresponding calculated force constants of butadiene, benzene, and biphenyl were scaled, with respect to experimental frequencies, by least-squares fitting as described in the Computational Methods section. The scaled force constants of terphenyl were obtained using scaling factors transferred from benzene and biphenyl.

In another approach, we use the calculated inter-ring stretching frequencies of pristine[20] and doped PPP (as defined as having a "pure" quinonoid structure) as well as those obtained from experiment.[22,46] The calculated frequencies are 1282 and 1450 cm^{-1} for pristine (aromatic) and doped (100% quinonoid) PPP, respectively. The experimental frequencies of pristine and highly doped sample are 1280 and 1328 cm^{-1}, respectively. We obtain the inter-ring C–C bond length using the following equation, which is a linear interpolation of inter-ring stretching frequency vs quinonoid structure:

$$r_{\text{inter-ring}} = r_A + f(r_Q - r_A)$$

where $f = (\Delta f_{expt}/\Delta f_{calc})$, Δf being the difference in inter-ring stretching frequencies of pristine and doped PPP; $r_{\text{inter-ring}}$ is the inter-ring C–C bond length; r_A is the calculated inter-ring bond length of the aromatic (pristine) PPP (from ref 38, 1.501 Å); r_Q is the calculated inter-ring bond length of "pure" quinonoid PPP (model Q, 1.365 Å). This estimate yields $r_{\text{inter-ring}} = 1.46$ Å, which is in excellent agreement with the value obtained using the relationship between force constants and bond lengths. From the value of f (~0.3), we are able to deduce that doped PPP has about 30% quinonoid character.

From the above results, we see a shortening of the inter-ring C–C bond going from pristine to doped PPP. Upon doping, the inter-ring C–C bond of PPP gains more bonding character and forms a bond resembling that of a benzene C–C bond (not a double bond). This result is consistent with X-ray crystallographic data on biphenyl anion[47] and terphenyl dianion.[48] As shown in Table 3, the inter-ring C–C bond lengths of biphenyl anion and terphenyl dianion are 1.435(5) and 1.42(3) Å, respectively. The ring unit comprises aromatic and double bond characters, resembling the structure of benzoquinone.[49] The evolution of the average structure of the repeat unit of PPP is summarized in Figure 9.

(46) Lefrant, S.; Buisson, J. P.; Eckhardt, H. *Synth. Met.* **1990**, *37*, 91.
(47) de Boer, E.; Klaassen, A. A. K.; Mooij, J. J.; Noordik, J. H. *Pure Appl. Chem.* **1979**, *51*, 73.
(48) Noordik, J. H.; Doesburg, H. M.; Prick, P. A. J. *Acta Crystallogr.* **1981**, *B37*, 1659.
(49) Trotter, J. *Acta Crystallogr.* **1960**, *86*, 86.

Table 3. Calculated Bond Lengths (Å) of the Repeat Unit of Pristine and Doped PPP: Comparisons with Experimental Data on Biphenyl and Terphenyl Bond Lengths

bond label[a]	calculated		experimental (X-ray diffraction)				
	pristine PPP	doped PPP	biphenyl[c]	biphenyl anion[d]	benzoquinone[e]	terphenyl[f]	terphenyl dianion[g]
a	1.501	1.45(2)[b]	1.495	1.435		1.505	1.42(4)
b	1.390	1.458	1.397	1.433	1.477	1.404	1.44(4)
c	1.378	1.334	1.390	1.379	1.322	1.404	1.39(4)

[a] See Figure 2 for bond labels. [b] Estimated from Figure 5. [c] Reference 53. [d] Reference 47. [e] Reference 49. [f] Reference 54. [g] Reference 48.

Pristine PPP Doped PPP

	Bond length (Å)	Force constant (mdyne/Å)	Bond length (Å)	Force constant (mdyne/Å)
a	1.5006	4.573	1.45(2)	5.475
b	1.3900	6.466	1.4575	5.455
c	1.3795	6.898	1.3345	8.111

Figure 9. Structural change of pristine PPP on doping, as adduced from this study. Upon doping, the inter-ring C–C bond gains bonding character and shortens to approximately 1.45 Å; the aromatic ring becomes quinonoid, resembling the structure of benzoquinone. See also Table 3 for data on geometries.

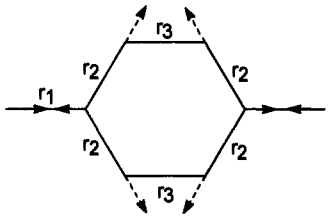

Figure 10. Internal coordinates of the $\Re_1$ mode. The arrows shown correspond to a unit cell plus the adjacent C atoms in the neighboring cells, which are in phase and correspond to k=0.

Raman Intensity. It is predicted by the effective conjugation coordinates (ECC) or $\Re$ mode theory[50-52] that the intensity ratio I_j/I_k of any two totally symmetrical modes (A_g modes) is given by

$$I_j/I_k = |L_{\Re j}|^2/|L_{\Re k}|^2$$

where $\Re_1$ is an internal coordinate (see Figure 10). $\Re_1$ in principle is the coordinate connecting the ground state with the electronic excited state of the molecule. While it is difficult to determine $\Re_1$ accurately, a plausible approximation can be defined as $\Re_1 = N(4\delta r_2 - \delta r_1 - 2\delta r_3)$, N being the normalizing factor. This approximation rests on the observation that the geometry of the electronically excited state of PPP is somewhat quinonoid, as depicted by Figure 10. $L_{\Re i}$ can be calculated from $L_{\Re} = \mathbf{BL}_x$, where $\mathbf{B}$ and $\mathbf{L}_x$ are matrices that transform the Cartesian displacement vector to $\Re$ and normal coordinates, respectively.

Using the above equation, we obtain the intensity ratios of the four A_g modes as shown in Table 4. These ratios are also compared to those calculated by the SQMOFF method and to those estimated from Raman spectrum reported in ref 22. It can be seen that both the $\Re$ mode theory and the SQMOFF method yield results that agree very well with the experimental result. These results illustrate the two following points.

Table 4. Intensity Ratios of the A_g Modes[a] Predicted by the $\Re$ Mode Theory and Calculated by the SQMOFF Method as Compared to Experimental Data[b]

	peaks[c]			
	A	B	C	D
$\Re$ mode	100	9	41	7
SQMOFF[d]	100	28	72	4
experimental	100	21	73	12

[a] Due to the uncertainty around the origin of peak D, the intensity ratio is taken with respect to peak A, which is given an arbitrary value of 100. [b] Calculated from Raman spectrum reported in ref 22. [c] See Figure 6 for labels. [d] Inter-ring scaling factor is 0.6000.

(1) The applicability of the $\Re$ mode theory for doped PPP. This could be associated with the correct assumption that the ground state structure of PPP is that of aromatic form and the excited state is that of quinonoid form, hence validating the definition of the $\Re_1$ mode. It appears that this $\Re_1$ mode is coupled to the A_g modes, and it lends intensity to these normal modes. In other words, an intensity dependency of A_g nodes on the $\Re_1$ mode—a mode which most strongly couples the geometry to the electronic structure—is observed.

(2) The soundness of the SQMOFF method as a reliable means of predicting the Raman spectrum in terms of both frequency and intensity. Further, the SQMOFF method also predicts that the intensity ratio I_B/I_C is also a measure of the quinonoid character in doped PPP. It can be seen from Figure 6 that I_B/I_C decreases with decreasing quinonoid character.

Conclusions

We present the first quantitative evidence of the structural change of PPP upon doping. This is accomplished by utilizing an integrated approach that combines theoretical and experimental methods. Based on the observed and calculated inter-ring stretching frequency increase, we estimate that doped PPP has about 30% quinonoid character and an inter-ring bond length of 1.46 Å. Furthermore, we also find an increase in inter-ring stretching force constant from 4.573 to 5.475 mdyn/Å upon doping. Using the relationship between force constants and bond lengths, we find that this increase corresponds to a decrease in the inter-ring C–C bond length from 1.501 to 1.45(2) Å.

We also established that the intensity ratios of the four strongest Raman peaks of doped PPP are dependent primarily on the quinonoid structure. This finding justifies the use of a neutral model, suitably capped to induce the correct structure, for simulation of the vibrational properties of doped PPP. Before this modeling concept can be generalized, further studies need to be done on other polymers.

From our past and present studies, we have established the soundness of the SQMOFF modeling method for both straight chain and ring polymers. In this study we show how this theoretical modeling method complements Raman spectroscopy in obtaining structural data not attainable otherwise. With this two-pronged approach, we provide a means of studying the doping-induced structural modification of a polymer when the X-ray diffraction technique is not applicable.

Acknowledgment. This work is supported by grants from NSF (DMR-91-15548) and the Pittsburgh Supercomputer Center (DMR-920006P).

(50) Zerbi, M.; Chierichetti, B. *J. Chem. Phys.* **1991**, *94*, 4637.
(51) Zerbi, G.; Gussoni, M.; Castigiloni, C. *Conjugated Polymers*; Kluwer Academic: the Neverthelands, 1991; pp 435.
(52) Castiglioni, C.; Gussoni, M.; Zerbi, G. *Synth. Met.* **1989**, *E1*, 29.
(53) Baudour, P. J. L.; Toupet, L.; Delugeard, Y.; Ghemid, S. *Acta Crystallogr.* **1986**, *C42*, 1211.
(54) Baudour, P. J. L.; Cailleau, H. *Acta Crystallogr.* **1977**, *B33*, 1773.
(55) Fauvarque, J. F.; Digua, A.; Petit, M. A.; Savard, J. *Makromol. Chem.* **1985**, *186*, 2415.